

**Deck model applied to baryonic systems\***

R. T. Cutler<sup>†</sup> and H. W. Wyld, Jr.

*Department of Physics, University of Illinois, Urbana, Illinois 61801*

(Received 12 June 1975)

Reggeized Deck model calculations are performed for the reactions  $p\bar{p} \rightarrow p\bar{p}\pi^+\pi^-$ ,  $pp \rightarrow pp\pi^+\pi^-$ , and  $pp \rightarrow pX$ . The calculations are compared with a new CERN-Serpukhov experiment at 25 and 40 GeV for the first reaction and with recent high-energy data from Fermilab and the CERN ISR for the other two reactions.

I. INTRODUCTION

In an earlier paper<sup>1</sup> (hereafter referred to as AW) a collaboration at the University of Illinois presented a Reggeized Deck model calculation for the reaction  $\pi^-p \rightarrow \pi^+\pi^-\pi^-p$ . The success of this model in providing detailed agreement with the data, including respectable agreement with the spin-parity structure of the data, has led us to reexamine Deck models for reactions where baryonic systems are formed. A further impetus was provided by the availability of new data<sup>2</sup> for the reaction  $p\bar{p} \rightarrow p\bar{p}\pi^+\pi^-$  at 25 and 40 GeV/c. The reactions  $p\bar{p} \rightarrow p\bar{p}\pi^+\pi^-$  and  $pp \rightarrow pp\pi^+\pi^-$  will be analyzed using techniques and assumptions analogous to those in AW, and detailed comparisons between theory and recent high-energy experiments will be made. In addition, the inclusive reaction  $pp \rightarrow pX$  will be examined in the spirit of the Reggeized Deck model and the results used to interpret some of the experimental data.

Reggeized Deck models for the reaction  $pp \rightarrow p\pi^-\Delta^{++}$  were first considered by Berger.<sup>3,4</sup> The Deck model for the reaction  $pp \rightarrow pn\pi^+$ , which dominates  $pp \rightarrow pX$  for low  $M_X$ , was also first studied by Berger.<sup>5</sup> More recently, extensive analyses of data at 6.6 GeV/c and comparisons with these models for both reactions have been performed by Colton *et al.*<sup>6,7</sup> Similar reactions have been considered by Wolf.<sup>8</sup> The reaction  $pp \rightarrow p\pi^-\Delta^{++}$  at 19 GeV/c was studied by Brink and Holmgren.<sup>9</sup> There is also an extensive Soviet literature which can be traced from the references in the paper by Boreskov, Kaidalov, and Ponomarev.<sup>10</sup>

Section II will present the model and method of calculation used for the reaction  $p\bar{p} \rightarrow p\bar{p}\pi^+\pi^-$ . The results of this calculation are compared to experiment in Sec. III. The reaction  $pp \rightarrow pp\pi^+\pi^-$  will be calculated and compared to experiment in Sec. IV. Section V will present an analysis of the inclusive reaction  $pp \rightarrow pX$ . We try to draw some general conclusions about the Deck model as applied to baryonic systems in Sec. VI.

II. MODEL

A. Diagrams considered

Three diagrams contributing to the reaction  $p\bar{p} \rightarrow p\bar{p}\pi^+\pi^-$  in the Reggeized Deck model will be considered; they are shown in Fig. 1. In these diagrams, a wiggly internal line represents a Regge-

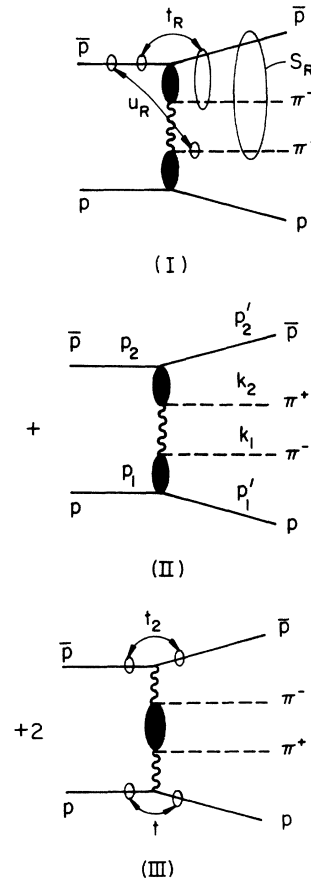


FIG. 1. Diagrams for  $p\bar{p} \rightarrow p\bar{p}\pi^+\pi^-$  calculated in this paper. The variables used to express the pion Regge trajectory are indicated schematically for diagram I and the labels used for 4-momenta are shown in II. Wiggly lines represent Reggeized pion exchanges. Shaded blobs represent complete elastic scattering amplitudes.

ized pion exchange, and a shaded blob refers to a full elastic scattering amplitude which contains, along with other components, the Pomeron trajectory. Since the elastic scattering considered always involves at least one pion,  $G$ -parity conservation implies that a shaded blob will not contain the pion trajectory. Thus, diagram III is entirely distinct from diagram I. Figure 2 shows three diagrams involving baryon exchange which will not be calculated because they are believed to be insignificant in the kinematic region of interest. Although I and II contain baryon exchange components inside the blobs, IV and V are distinct from I and II, again because the blobs do not contain the pion trajectory. The cross-hatched blob in VI can contain pion exchange as well as Pomeron exchange, and thus a small part of this diagram is contained in I and II.

### B. Component pieces of the Deck amplitude

Diagrams I and II are exactly analogous to the  $3\pi$  production diagram considered in AW, and will be calculated in the same way insofar as possible. Diagram III is treated in the same spirit, using the  $ig\gamma_5$  coupling for the  $NN\pi$  vertices, where  $g^2/4\pi = 14.5$ . The amplitude in this model for the reaction  $p\bar{p} \rightarrow p\bar{p}\pi^+\pi^-$  is

$$\begin{aligned} \mathfrak{M} &= \mathfrak{M}_I + \mathfrak{M}_{II} + 2\mathfrak{M}_{III}, \\ \mathfrak{M}_I &= \mathfrak{M}_{\alpha\beta}(\pi^-\bar{p} \rightarrow \pi^-\bar{p}) \mathfrak{R}_\pi(t_{R1}, s_{R1}, u_{R1}) \mathfrak{M}_{\delta\gamma}(\pi^+p \rightarrow \pi^+p), \\ \mathfrak{M}_{II} &= \mathfrak{M}_{\alpha\beta}(\pi^+\bar{p} \rightarrow \pi^+\bar{p}) \mathfrak{R}_\pi(t_{R2}, s_{R2}, u_{R2}) \mathfrak{M}_{\delta\gamma}(\pi^-p \rightarrow \pi^-p), \\ \mathfrak{M}_{III} &= -g^2 \bar{v}_\beta(p_2) \gamma_5 v_\alpha(p'_2) \mathfrak{R}_\pi(t_2, s_{R4}, u_{R4}) \\ &\quad \times \mathfrak{M}(\pi^0\pi^0 \rightarrow \pi^+\pi^-) \mathfrak{R}_\pi(t, s_{R3}, u_{R3}) \bar{u}_\delta(p'_1) \gamma_5 u_\gamma(p_1). \end{aligned} \quad (1)$$

The Reggeized propagator,  $\mathfrak{R}_\pi$ , is taken to be exactly that used in AW. It is, then,

$$\mathfrak{R}_\pi(t, s, u) = \frac{[(s-u)/2s_0]^{\alpha_\pi(t)} e^{-i(\pi/2)\alpha_\pi(t)}}{m_\pi^2 - t_R}, \quad (2)$$

with

$$\begin{aligned} \alpha_\pi(t) &= t - m_\pi^2, \\ s_0 &= 1 \text{ GeV}^2. \end{aligned} \quad (3)$$

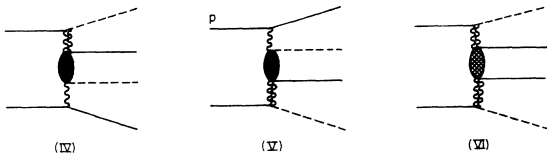


FIG. 2. Deck-like diagrams not calculated in this work. Double wiggly lines refer to baryon trajectories. Solid external lines are nucleons, dashed lines are pions.

In terms of 4-momenta, the kinematic variables used in the Reggeized propagators are

$$\begin{aligned} s_{R1} &= s_{R2} = s_{R4} = W^2 = (p'_2 + k_1 + k_2)^2, \\ t_{R1} &= (p'_2 + k_1 - p_2)^2, \quad t_{R2} = (p'_2 + k_2 - p_2)^2, \\ u_{R1} &= (k_2 - p_2)^2, \quad u_{R2} = (k_1 - p_2)^2, \\ t &= (p'_1 - p_1)^2, \quad t_2 = (p_2 - p'_2)^2, \\ u_{R3} &= (k_1 + k_2 - p_1)^2, \quad u_{R4} = (k_1 + k_2 - p_2)^2, \\ s_{R3} &= W_2^2 = (p'_1 + k_1 + k_2)^2. \end{aligned} \quad (4)$$

The choice of these variables is, as in AW, considered appropriate for small  $W$ . In this kinematic region the  $\pi\bar{p}$  scattering in the upper vertices of I and II should be dominated by resonance production, and the  $\pi p$  amplitude of the lower vertex by Pomeron exchange. Thus, one imagines that the Reggeized pion is being exchanged in the process  $P\bar{p} \rightarrow \pi\bar{N}^*$ , with  $P$  the Pomeron and  $\bar{N}^*$  a resonant state to be treated as a particle, and uses the appropriate kinematic variables. Similarly, the  $2\pi$  system in III is constrained to have low mass for small  $W$ , and is also presumed to be dominated by resonances. Further discussion of this point can be found in AW.

Fits to the experimental data are used for the elastic scattering amplitudes  $\mathfrak{M}(\pi N \rightarrow \pi N)$  and  $\mathfrak{M}(\pi\pi \rightarrow \pi\pi)$ , and AW has a lengthy discussion of the amplitudes used. Briefly,  $\mathfrak{M}(\pi\pi)$  is based primarily on the partial-wave fit of Protopopescu *et al.*,<sup>11</sup> and the low-energy part of  $\mathfrak{M}(\pi N)$  on the CERN 1967 partial-wave analysis.<sup>12</sup> For high energies ( $M_{\pi N} \gtrsim 2 \text{ GeV}$ ), the Regge-pole fit of Barger and Phillips<sup>13</sup> is used. Baryon exchange components are not included in this high-energy region.

### C. On-shell amplitudes

As in AW, on-shell amplitudes are used for both  $\pi N$  and  $\pi\pi$  scattering; no off-shell mass extrapolation form factors are introduced. To quote from AW, "We have adopted this on-shell philosophy because we feel that the theoretical uncertainties involved in off-shell extrapolations are as great as the theoretical uncertainties in using the Deck model to begin with." Unfortunately, as this project developed, it rapidly became apparent that there are at least two sensible ways to use on-shell amplitudes for  $\pi N$  scattering. The approach taken in AW is to write

$$\begin{aligned} \mathfrak{M}_{\alpha\beta}(\pi^-\bar{p}) &= \mathfrak{M}_{\alpha\beta}(\pi^+p) \\ &= \bar{u}_\alpha(p'_2) (\mathfrak{G}_{+u} + \mathfrak{G}_{+u} \not{k}_1) u_\beta(p_2), \end{aligned} \quad (5)$$

where, to be explicit, the amplitude for the upper vertex of I has been written, using charge-con-

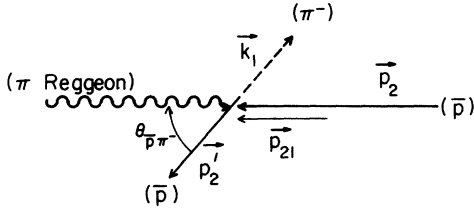


FIG. 3. Kinematic diagram for the upper vertex of diagram I, showing the c.m. scattering angle  $\theta_{\bar{p}\pi^-}$  and  $\vec{p}_{21}$ , the vector used in on-shell amplitudes.

jugation invariance. The subscripts on  $\mathcal{G}$  and  $\mathcal{B}$  refer to the charge of the pion (+ or -) and the vertex (upper or lower). The prescription used in AW is to take the invariant amplitudes  $\mathcal{G}_{+u}$  and  $\mathcal{B}_{+u}$  as functions only of energy and center-of-mass scattering angle,  $\mathcal{G}_{+u} = \mathcal{G}_{\pi^+\bar{p}}(M_{\bar{p}\pi^-}, \cos\theta_{\bar{p}\pi^-})$ . Figure 3 shows how  $\theta_{\bar{p}\pi^-}$  is defined. In an effort to include as much information as possible about the actual off-shell process, the wave functions  $\bar{u}_\alpha(p'_2)$ ,  $u_\beta(p_2)$  are used. This prescription, sensible as it seems, leads to serious disagreement with experimental data, especially if one looks at angular distributions in the upper vertex center of mass. The dashed curve in Fig. 4 shows the distribution in  $\cos\theta_{\bar{p}\pi^-}$  resulting from this on-shell prescription (details of calculation will be presented later) compared with experiment<sup>2</sup> for small  $W$ . The shape of the curve is very different from the data, and the total cross section is too large. The same effect is seen if different  $W$  cuts are made, although the problem is less severe for high  $W$ . The reason for this is clear; when  $M_{\bar{p}\pi^-}$  is large the prescription used to go on-shell is not important. In AW, of course,  $\pi N$  scattering occurs only at the lower vertex, where  $M_{p\pi}$  is quite large.

There is another sensible way to use on-shell amplitudes. The entire amplitude  $\mathfrak{M}_{\alpha\beta}(\bar{p}\pi)$ , instead of  $\mathcal{G}$  and  $\mathcal{B}$ , may be considered a function only of  $M_{\bar{p}\pi}$  and  $\cos\theta_{\bar{p}\pi}$ . This corresponds to taking

$$\mathfrak{M}_{\alpha\beta}(\pi^-\bar{p}) = \bar{u}_\alpha(p'_2)(\mathcal{G}_{+u} + \mathcal{B}_{+u}\not{k}_1)u_\beta(p_{21}), \quad (6)$$

where

$$\vec{p}_{21} = |\vec{p}'_2| \frac{\vec{p}_2}{|\vec{p}_2|}, \quad p_{21}^2 = p_2^2 = M^2, \quad (7)$$

#### D. Spin sums

The amplitudes involved, then, can be written

$$\begin{aligned} \mathfrak{M}_I &= \bar{u}_\alpha(p'_2)(\mathcal{G}_{+u} + \mathcal{B}_{+u}\not{k}_1)u_\beta(p_{21})\mathcal{R}_{\pi_1}\bar{u}_\delta(p'_1)(\mathcal{G}_{+l} + \mathcal{B}_{+l}\not{k}_2)u_\gamma(p_{11}), \\ \mathfrak{M}_{II} &= \bar{u}_\alpha(p'_2)(\mathcal{G}_{-u} + \mathcal{B}_{-u}\not{k}_2)u_\beta(p_{22})\mathcal{R}_{\pi_2}\bar{u}_\delta(p'_1)(\mathcal{G}_{-l} + \mathcal{B}_{-l}\not{k}_1)u_\gamma(p_{12}), \\ \mathfrak{M}_{III} &= -g^2 u_\alpha(p'_2)\gamma_5 u_\beta(p_2)\mathcal{R}_{\pi_4}\mathfrak{M}(\pi\pi)\mathcal{R}_{\pi_3}\bar{u}_\delta(p'_1)\gamma_5 u(p_1). \end{aligned} \quad (8)$$

The spin sums can be done most easily by trace techniques. The diagonal terms  $|\mathfrak{M}_i|^2$  present no diffi-

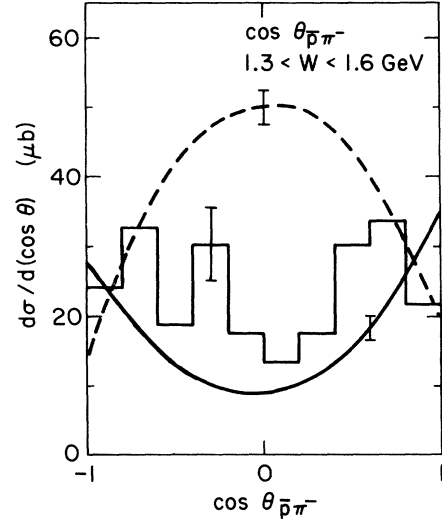


FIG. 4. Distribution in  $\cos\theta_{\bar{p}\pi^-}$ , where  $\theta_{\bar{p}\pi^-}$  is the scattering angle of the  $\bar{p}$  in the  $\bar{p}\pi^-$  center-of-mass system, for the reaction  $p\bar{p} \rightarrow p\bar{p}\pi^+\pi^-$  at  $p_L = 25$  GeV/c.  $W$  has been restricted to  $1.3 < W < 1.6$  GeV, and  $t$  to  $0.05 < -t < 0.3$  GeV<sup>2</sup>. The two theoretical curves differ in the prescription for using on-mass-shell amplitudes, as explained in the text. The experimental data are from the CERN-Serpukhov spectrometer experiment (Ref. 2).

as shown schematically in Fig. 3. In (6)  $\mathcal{G}$  and  $\mathcal{B}$  are considered functions of  $M_{\bar{p}\pi^-}$  and  $\cos\theta_{\bar{p}\pi^-}$  as before. The expedient of defining  $p_{21}$  (and in a similar manner  $p_{11}$ ,  $p_{22}$ , and  $p_{12}$ ) may appear clumsy, but it allows one to use tables of the invariant amplitudes  $\mathcal{G}$  and  $\mathcal{B}$ , and to keep the phase information necessary to calculate  $|\mathfrak{M}_I + \mathfrak{M}_{II}|^2$  without ignoring the cross term. The solid curve in Fig. 4 shows the distribution in  $\cos\theta_{\bar{p}\pi^-}$  resulting from this prescription for using on-shell amplitudes. The agreement with data is improved, and this method of using on-shell amplitudes will be used henceforth for  $\mathfrak{M}(\pi N)$ .

In the same spirit, but with some trepidation since both incoming particles are off-shell,  $\mathfrak{M}(\pi^0\pi^0 \rightarrow \pi^+\pi^-)$  is taken to be a function only of  $M_{\pi\pi}$  and  $\cos\theta_{\pi\pi}$ , where  $\theta_{\pi\pi}$  is measured in the  $\pi\pi$  center-of-mass system, and is defined by the 3-momenta of the particles and Reggeons involved.

culties, but in the cross terms one meets objects like  $u_\beta(p_{22})\bar{u}_\beta(p_{21})$ . This can be expressed as

$$\begin{aligned} \sum_{\text{spins } \beta} u_\beta(p_{22})\bar{u}_\beta(p_{21}) &= \frac{m_p + \not{p}_{22}}{(m_p + E_{22})^{1/2}} \sum_{\beta} u_\beta(0) \frac{m_p + \not{p}_{21}}{(m_p + E_{21})^{1/2}} \bar{u}_\beta(0) \\ &= \frac{m_p + \not{p}_{22}}{(m_p + E_{22})^{1/2}} \left( \frac{1 + \gamma_0}{2} \right) \frac{m_p + \not{p}_{21}}{(m_p + E_{21})^{1/2}}, \end{aligned} \quad (9)$$

and the cross term between  $\mathfrak{M}_I$  and  $\mathfrak{M}_{II}$  becomes

$$\begin{aligned} \frac{1}{4} \sum_{\text{spins}} 2 \operatorname{Re}(\mathfrak{M}_{II} \mathfrak{M}_I^*) &= \frac{1}{2} \operatorname{Re} \left[ \operatorname{Tr} \left( (\not{p}'_2 + m_p)(\mathfrak{G}_{-u} + \mathfrak{G}_{-u} \not{p}'_2) \frac{\not{p}_{22} + m_p}{(E_{22} + m_p)^{1/2}} \frac{1 + \gamma_0}{2} \frac{\not{p}_{21} + m_p}{(E_{21} + m_p)^{1/2}} (\mathfrak{G}_{+u}^* + \mathfrak{G}_{+u}^* \not{p}'_1) \right) \right. \\ &\quad \left. \times \operatorname{Tr} \left( (\not{p}'_1 + m_p)(\mathfrak{G}_{-I} + \mathfrak{G}_{-I} \not{p}'_1) \frac{\not{p}_{12} + m_p}{(E_{12} + m_p)^{1/2}} \frac{1 + \gamma_0}{2} \frac{\not{p}_{11} + m_p}{(E_{11} + m_p)^{1/2}} (\mathfrak{G}_{+I}^* + \mathfrak{G}_{+I}^* \not{p}'_2) \right) \right]. \end{aligned} \quad (10)$$

The evaluation of this expression was greatly facilitated by the use of the algebra program ASHMEDAI,<sup>14</sup> developed by Levine. Each trace generates 76 terms, a typical term being  $E_1'(p_{11} \cdot p_{12})(k_1 \cdot k_2)$ . The cross term between  $(\mathfrak{M}_I + \mathfrak{M}_{II})$  and  $\mathfrak{M}_{III}$  can be evaluated in the same way.

### E. Calculation

The cross section for  $p\bar{p} \rightarrow p\bar{p}\pi^+\pi^-$  can be written

$$\begin{aligned} d\sigma &= \frac{1}{(2\pi)^8} \frac{1}{2^9} \frac{2\pi}{(p_L m_p)^2} \\ &\quad \times \left( \frac{1}{4} \sum_{\text{spins}} |\mathfrak{M}_I + \mathfrak{M}_{II} + \mathfrak{M}_{III}|^2 \right) d^7\tau, \\ d^7\tau &= \frac{dW}{W} dt d\alpha d\cos\beta d\gamma ds_1 ds_2, \end{aligned} \quad (11)$$

where the variables used to express phase space are the same as in AW:  $W = M_{\bar{p}\pi\pi}$  is the three-particle mass;  $t$  is the momentum transfer to the proton;  $\alpha, \cos\beta, \gamma$  are three Euler angles describing the orientation of the  $\bar{p}\pi\pi$  system; and  $s_1, s_2$  are the Dalitz-plot variables  $M_{\bar{p}\pi}^2$  and  $M_{\bar{p}\pi^+}^2$ . As in AW, the cross section is evaluated by a Monte Carlo technique. The calculation generates a random sample of  $p\bar{p}\pi\pi$  events which are distributed according to  $d\sigma/d^7\tau$ . Typically, between 20 000 and 30 000 events are generated, and these events can be analyzed in exactly the same way one would treat experimental data. Histograms are made of various distributions and smooth curves drawn through the points. Error bars appearing on the theoretical curves of some figures will reflect statistical error associated with the finite number of events generated. The greatest advantage of this Monte Carlo approach is that the distribution of any variable may be easily displayed in any kinematic region and compared directly with experimental data.

## III. RESULTS

### A. Comparison with data

The calculation was performed at lab momenta of 25 and 40 GeV/c, in order to compare to the data of Ref. 2. In order to compare the scale as

well as the shape of theoretical and experimental distributions, it is necessary to display experimental histograms in terms of cross section as opposed to number of events. The most reliable conversion factors (expressed as  $\mu\text{b}/\text{event}$ ) are found from the cross sections reported in Ref. 2 for  $0.05 < -t < 0.3 \text{ GeV}^2$ . Thus, the experimental histograms are scaled in such a way that  $\sigma(0.05 < -t < 0.3 \text{ GeV}^2, W < 2.2 \text{ GeV})$  is  $166 \mu\text{b}$  at 25 GeV/c and  $149 \mu\text{b}$  at 40 GeV/c. All distributions for the reaction  $p\bar{p} \rightarrow p\bar{p}\pi^+\pi^-$  will be displayed with  $t$  limited to this range. Acceptance corrections have been included in the experimental histograms, and error bars reflect statistical errors only.

### B. Three-particle mass distributions

Figure 5 shows differential cross sections in  $W$  for the two lab momenta. The broken curves show the contributions of the three diagrams and the cross term between diagrams I and II. The relative importance of I, II, and the cross term are approximately independent of lab momentum, whereas III decreases rapidly with increasing momentum. The cross term between (I + II) and III is very small, and, to save computer time, was not included in the calculations presented.

The agreement between this calculation and experiment is quite reasonable at 40 GeV/c if one interprets the experimental distribution to be the sum of a Deck-model background and certain resonancelike structures. This interpretation seems to indicate the existence of two resonances with masses of about 1.45 GeV and 1.72 GeV. We hasten to add that the authors of Ref. 2 (where the experimental data are presented) claim the bump at 1.45 GeV has little or no statistical significance and that the angular distributions in this region do not show the structure associated with a single resonance. Nevertheless, there does not seem to be

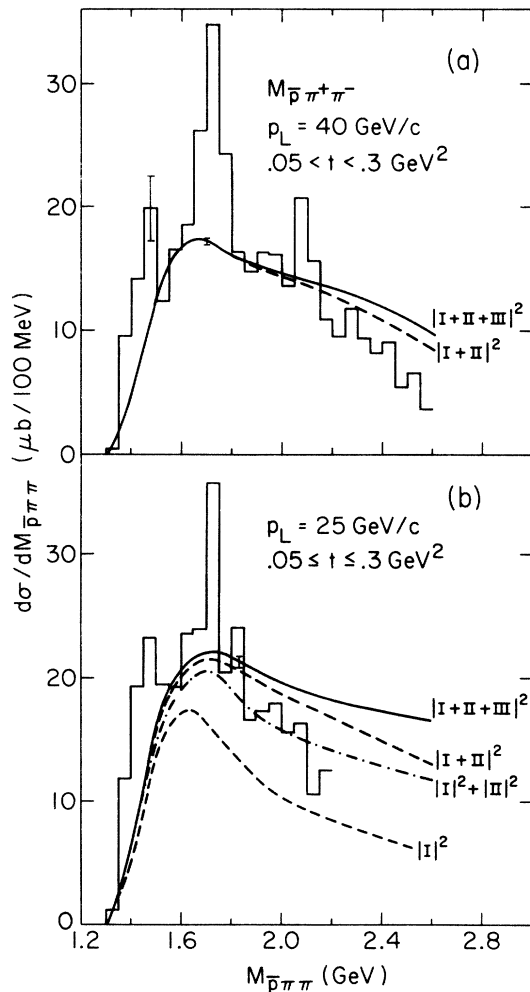


FIG. 5. Distribution in  $W = M_{\bar{p}\pi^+\pi^-}$  for the reaction  $p\bar{p} \rightarrow p\bar{p}\pi^+\pi^-$ . The contributions of various parts of the Deck amplitude are shown as broken lines. Lab momentum is (a) 40 GeV/c, (b) 25 GeV/c. Experimental data are not presented in (a) and (b) for  $W$  greater than 2.6 and 2.2 GeV, respectively, because the acceptance corrections are not considered reliable for high  $W$ . This matter is discussed in Ref. 2. The experimental data are from the CERN-Serpukhov spectrometer experiment (Ref. 2).

any reasonable modification of the Deck model in this exclusive process that will allow the low mass data to be entirely ascribed to a Deck mechanism. The Deck cross section appears to insist on peaking above 1.6 GeV, and tinkering with the model typically only affects the rate of decline above this mass. (As will be discussed later, there is a Deck-like diagram for the reaction  $p\bar{p} \rightarrow p\bar{p}\pi$  which gives a large peak at missing mass roughly 1.4 GeV, but this is irrelevant for the reaction  $p\bar{p} \rightarrow p\bar{p}\pi\pi$ .)

In contrast to this uncertain situation for low

$W$ , the resonance character of the bump at about 1.72 GeV is reasonably well established; the mass spectrum presented in the data of Ref. 2 shows a clearly resolved bump, and angular distributions in this region have structure consistent with a baryon resonance decaying to  $\Delta\pi$ .

The experimental cross section seems to drop off at high  $W$  somewhat faster than this Deck model predicts, although the discrepancy seems to be confined to  $W > 2.2$  GeV. It should perhaps be emphasized that there are no free parameters in this model. In particular, if the normalization were free one could obtain a much better looking fit to experiment by moving the theory curve down a bit. The same effect results from using a different total cross section for the data; the uncertainty in cross section is stated in Ref. 2 to be about 6% statistical and 10% systematic at 40 GeV/c. Thus, the normalization of the experimental histogram has the same uncertainty.

Theory and experiment do not agree as well at 25 GeV/c. The low-mass structure looks much the same, with resonancelike bumps in the data appearing at about 1.45 and 1.72 GeV. However, the experimental cross section falls well below theory above  $W = 1.85$  GeV. The problem may, of course, be with the model used. We feel that the calculation of diagram III is not as reliable as the other diagrams, both because an on-shell amplitude has been used for a process with *two* particles off-shell, and because the vertex factor  $ig\gamma_5$  probably should be modified by a form factor (see Sec. V). However, completely eliminating III clearly does not reconcile theory and experiment at either energy. Although it is, of course, possible that this problem indicates a real failing of the Deck model, it should be remembered that acceptance corrections of the data increase for high  $W$  (cf., Fig. 1 of Ref. 2), and that the authors of Ref. 2 do not consider this correction reliable for  $W$  above 2.6 (2.2) GeV at lab momentum 40 (25) GeV/c.

### C. Other distributions

Various spectra will now be displayed at 40 GeV/c. The comparison between theory and experiment is similar for 25 GeV/c, but we feel that both theory and experiment are more reliable at 40 GeV/c; the calculation has less contribution from diagram III at 40 GeV/c, and the data for  $W < 2.2$  GeV have a smaller acceptance correction.

Two-particle mass distributions are shown for  $1.3 < W < 2.2$  GeV in Fig. 6. There do not appear to be any serious discrepancies between experiment and theory in the shapes of these distributions.

The agreement between theory and experiment is generally less good for angular variables (or, equivalently, momentum transfers) than it is for two- or three-particle masses. These spectra will be displayed in three regions of  $W$ :  $1.3 < W < 1.6$  GeV (low  $W$ ),  $1.6 < W < 1.8$  GeV (medium  $W$ ), and  $1.8 < W < 2.2$  GeV (high  $W$ ). Examination of Fig. 5(a) suggests that the experimental distributions may be complicated by resonances in the low- $W$  and medium- $W$  regions, but that there is possibly only one important resonance in each region. One might hope for the best agreement between theory and experiment for high  $W$ , al-

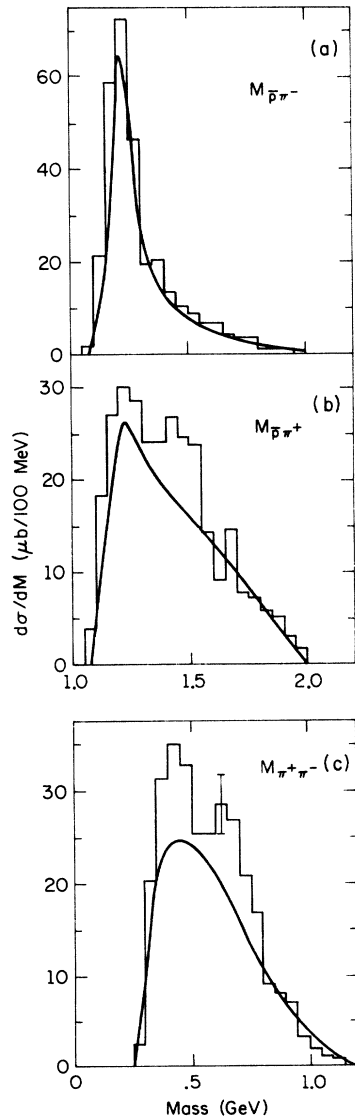


FIG. 6. Two-particle mass spectra for  $p\bar{p} \rightarrow p\bar{p}\pi^+\pi^-$  at  $p_L = 40$  GeV/c, with  $1.3 < W < 2.2$  GeV,  $0.05 < -t < 0.3$  GeV<sup>2</sup>. The experimental data are from the CERN-Serpukhov spectrometer experiment (Ref. 2).

though the calculation in AW was slightly less successful for high  $W$  ( $A_3$  region) than for low  $W$  ( $A_1$  region). Much of the following discussion will tacitly assume that diagram I, with its  $\Delta^{--}$  production is strongly dominant.

The Gottfried-Jackson angle,  $\theta_{GJ}$ , is displayed in Fig. 7. This is defined as the angle between the incoming  $\bar{p}$  and the  $(\bar{p}\pi^-)$  system in the  $\bar{p}\pi\pi$  center-of-mass system. This angle is a natural variable to use if one is considering the decay  $N^* \rightarrow \Delta^{--}\pi^+$ . There is, unfortunately, some disagreement between theory and experiment for high  $W$ . This problem will be discussed later, when  $t_{R1}$  is displayed. The most difference, however, is encountered for medium  $W$ , where there is apparently a large resonance contribution. We will resist the temptation to speculate on the spin-parities of resonances which may be involved in this reaction. To unravel this information, as well as which decay modes are important, would presumably require examination of other angular

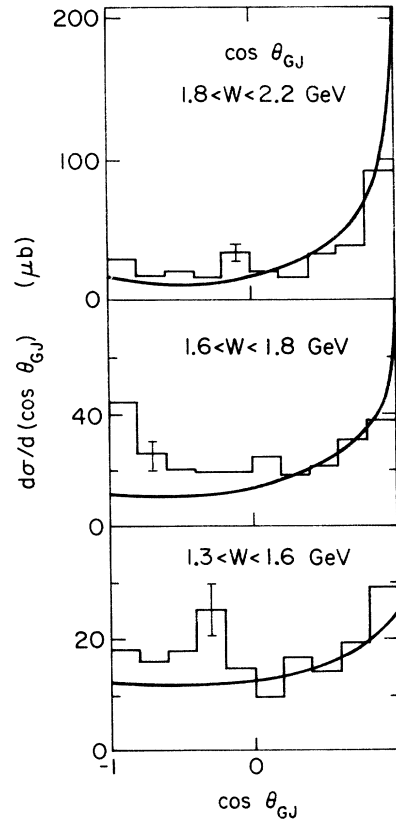


FIG. 7. Gottfried-Jackson angle for  $p\bar{p} \rightarrow p(\bar{p}\pi^+)\pi^+$  at  $p_L = 40$  GeV/c, with  $0.05 < t < 0.3$  GeV<sup>2</sup>.  $\theta_{GJ}$  is the angle between the incoming  $\bar{p}$  and the  $(\bar{p}\pi^-)$  system in the  $\bar{p}\pi\pi$  center-of-mass system. The experimental data are from the CERN-Serpukhov spectrometer experiment (Ref. 2).

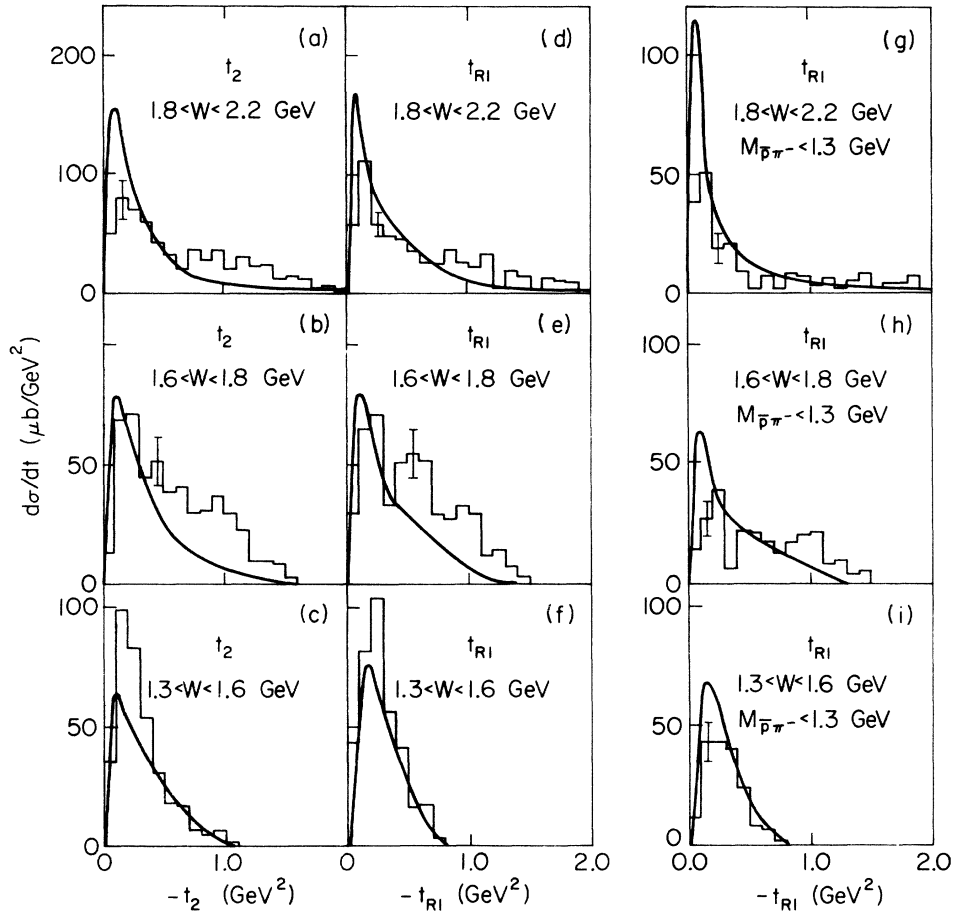


FIG. 8. Momentum-transfer distributions for  $p\bar{p} \rightarrow p\bar{p}\pi^+\pi^-$  at  $p_L = 40$  GeV/c, with  $0.05 < -t < 0.3$  GeV<sup>2</sup>: (a)–(c)  $t_2$ , the momentum transfer to the  $\bar{p}$ , (d)–(f)  $t_{R1}$ , the momentum transfer between the incident  $\bar{p}$  and the  $(\bar{p}\pi^-)$  system, (g)–(i)  $t_{R1}$ , with the  $(\bar{p}\pi^-)$  mass restricted to the  $\Delta(1236)$  rggion. The experimental data are from the CERN–Serpukhov spectrometer experiment (Ref. 2).

variables. Also, we feel that neither the calculation nor the data is sufficiently accurate to justify subtracting the theory, regarded as a background, from the data. However, it seems worthwhile to point out that the comparison of data and theory in the medium- $W$  range indicates the possibility of an interference term between resonance and Deck consistent with a resonance amplitude proportional to  $\cos\theta_{GJ}$ . Looking only at the data, which is very symmetric, one would probably not consider such a term.

Figure 8 shows distributions in  $t_{R1}$  and  $t_2$  (the momentum transfer at the upper vertex) for the three regions of  $W$ . Since  $t_{R1}$  is the momentum transfer associated with  $\theta_{GJ}$ , Figs. 8(d)–8(f) contain essentially the same information as Fig. 7. In particular, for high  $W$  the theoretical curve has a higher peak than the data, and is lower than the data for  $-t_R \geq 0.8$  GeV<sup>2</sup>. Figures 8(g)–8(i) show the same momentum transfer with the  $\bar{p}\pi^-$  mass

constrained to the  $\Delta(1236)$  region. As pointed out in Sec. II, the Regge parametrization used in diagram I is most appropriate if the  $\bar{p}\pi^-$  system is a resonant state. Thus, restricting  $M_{\bar{p}\pi^-}$  to the  $\Delta$  region may be expected to improve the approximations inherent in this model. Although the theoretical peak at low  $t_{R1}$  is still much larger than the experiment in Fig. 8(g), it is interesting that experiment and theory now agree well for large  $t_{R1}$ .

The agreement between theory and experiment in Fig. 8 for  $t_2$  is not very good. This variable is, of course, directly related to  $\theta_{\bar{p}\pi^-}$ , and thus is, as shown in Fig. 4, extremely sensitive to the way in which on-shell amplitudes are used. The distributions in  $t_2$  could presumably be changed by altering this prescription or by including an off-shell form factor. Unfortunately, such modifications also affect the  $t_R$  distributions, and it is a bit hard to decide just how one wants to change these spectra. How does one decide that a dis-

TABLE I. Slope  $b$  of the differential cross section  $d\sigma/dt \sim e^{bt}$ , for  $0.05 < -t < 0.3 \text{ GeV}^2$ , for the reaction  $p\bar{p} \rightarrow p\bar{p}\pi^+\pi^-$ .

$W$ (GeV)	$b$ ( $\text{GeV}^{-2}$ )			
	25 GeV/c		40 GeV/c	
	Th	Exp	Th	Exp
1.3–1.6	$10.8 \pm 0.3$	$12.4 \pm 1.1$	$11.5 \pm 0.3$	$15.7 \pm 1.5$
1.6–1.8	$9.8 \pm 0.4$	$8.1 \pm 0.9$	$10.2 \pm 0.3$	$6.6 \pm 0.9$
1.8–2.2	$8.6 \pm 0.4$	$5.2 \pm 0.8$	$8.8 \pm 0.3$	$5.8 \pm 0.9$

crepancy between theory and experiment is due to a problem in the model and not resonant structure in the data?

Table I shows the slope of  $\ln(d\sigma/dt)$  in the three ranges of  $W$ . Although the values of  $b$  predicted by the Deck model show the same trend as the experimental slopes to decrease as  $W$  increases, the effect is obviously more dramatic in the data. Roughly the same situation is observed in the Deck calculation<sup>1,15</sup> of  $\pi p \rightarrow 3\pi p$ . Figure 9 shows the dependence of the slope parameter  $b$  on the  $3\pi$  mass  $W$  for this latter reaction. There is a clear discrepancy between the experimental data<sup>16</sup> and the Deck-model calculation from AW. It is very difficult to see any simple resolution to this problem in the context of a Deck mechanism. One might try to resolve the problem by including an off-mass-shell form factor  $F(t, t_R)/F(t, m_\pi^2)$  in the  $\pi N$  scattering amplitudes. For example,  $\exp[at(t_R - m_\pi^2)]$  might be considered. However, the requirement

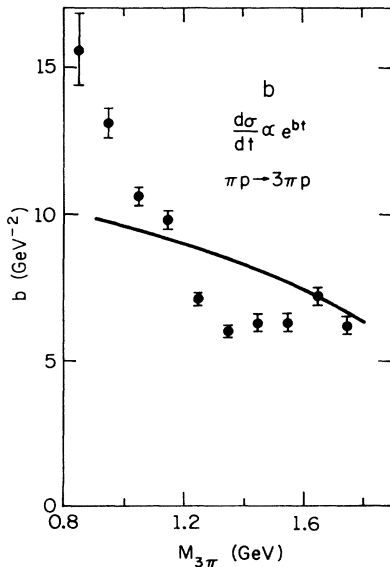


FIG. 9. Slope  $b$  of the cross section  $d\sigma/dt \propto e^{bt}$  for the reaction  $\pi^- p \rightarrow \pi^+ \pi^- \pi^- p$ . Experimental points (Ref. 16) are for the combined 11–25-GeV/c data. The theoretical curve is for the 16-GeV/c calculation of AW (Ref. 1).

that  $F$  be unity when the internal particle has the pion mass makes it very unlikely that this exponent can help. At low  $W$ ,  $t_R$  is kinematically constrained to be small (and thus near the pion mass), but the  $t$  dependence of experiment and theory disagree at small  $W$ . Thus, the  $W$  dependence of  $b$  cannot be ascribed to such a form factor unless the  $t_R$  dependence of  $F$  is almost discontinuous.

#### IV. REACTION $pp \rightarrow pp\pi^+\pi^-$

Changing the incident antiproton into a proton is simple in the model considered here. One simply replaces  $(\mathcal{G}_{+u} - \mathcal{G}_{-u})$ ,  $(\mathcal{G}_{-u} - \mathcal{G}_{+u})$ ,  $(\mathcal{G}_{+u} - \mathcal{G}_{-u})$ ,  $(\mathcal{G}_{-u} - \mathcal{G}_{+u})$  in Eqs. (8) and (10). This yields a model which does not treat the two protons in the final state as identical particles. In the kinematic region considered, however, this is an excellent approximation; if an event has  $t$  and  $t_2$  small enough for the Deck amplitude to be non-negligible, exchange diagrams will have very large momentum transfers at both vertices, and can be ignored. There are also difficulties involved when the incident energy is not high enough to separate the target fragmentation and projectile fragmentation regions. If  $W$  and  $W_2$  [see Eq. (4)] are comparable, with which proton does one associate the  $2\pi$  system in the Regge parametrization? Such problems will be avoided by presenting calculations of this reaction only for lab momentum greater than 50 GeV/c, with kinematic constraints such that  $W$  is clearly less than  $W_2$ .

The general features of this model are quite similar to that used by Boreskov *et al.*<sup>10</sup> to cal-

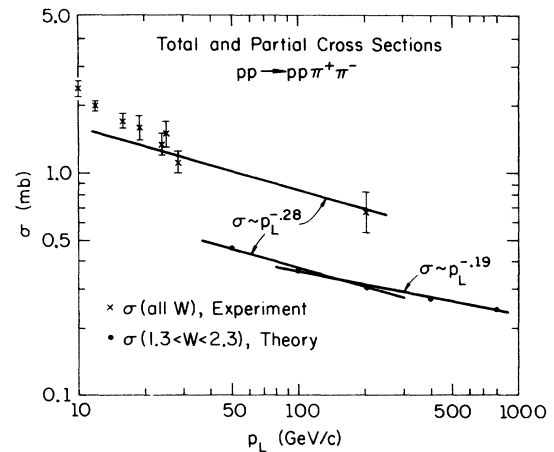


FIG. 10. Cross section as a function of lab momentum for the reaction  $pp \rightarrow pp\pi^+\pi^-$ . Experimental points (Refs. 17, 18, 19, 20) are total cross sections. Theoretical points are cross sections for the range  $1.3 < W < 2.3$  GeV. Thus, only the  $p_L$  dependence of experiment and theory should be compared, not the absolute size of the cross sections.

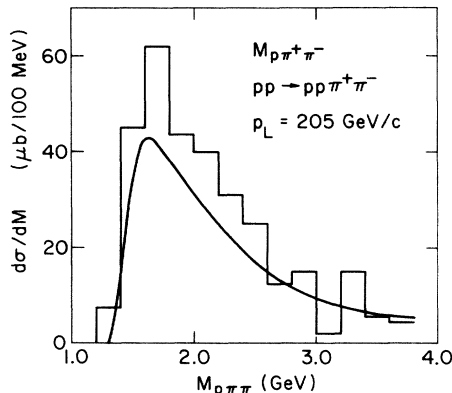


FIG. 11. Distribution in  $W = M_{p\pi\pi}$  for the reaction  $pp \rightarrow pp\pi^+\pi^-$  at 205 GeV/c. The experimental histogram is taken from Ref. 17.

culate the same reaction. There are, however, significant differences in the details of the model and the method of calculation: (1) Boreskov uses a phenomenological form factor for off-shell amplitudes; (2) the forms used for the Regge propagators are quite different in the two models; (3) Boreskov has four free parameters (three for the Regge parametrization and one for the off-shell form factor), whereas all parameters in our model have been determined from analysis of other reactions; (4) we calculate the cross term between diagrams I and II, ignored in Ref. 10, and find it to be significant.

Figure 10 shows the dependence of cross section on the lab momentum of the incident proton. The

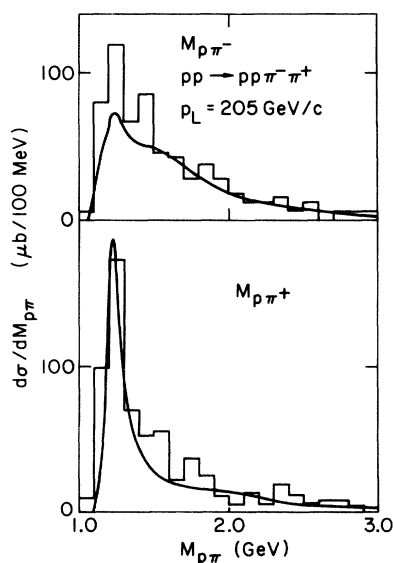


FIG. 12. Two-particle mass spectra for  $pp \rightarrow pp\pi^+\pi^-$  at 205 GeV/c. The experimental histograms are taken from Ref. 17.

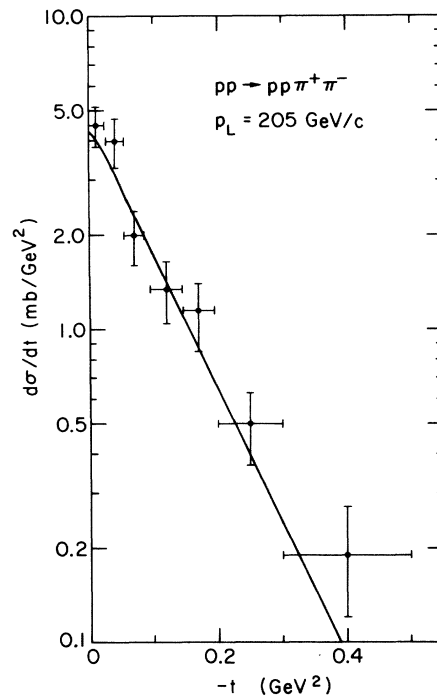


FIG. 13. Momentum transfer to the proton for the reaction  $pp \rightarrow pp\pi^+\pi^-$  at 205 GeV/c. The experimental points are taken from Ref. 17.

theoretical points are calculated by the usual Monte Carlo technique for  $1.3 < W < 2.3$  GeV. The experimental points<sup>17-20</sup> are total cross sections; no  $W$  cut has been made on the data. Thus, the size of theoretical and experimental cross sections are not directly comparable. One may, however, compare the dependence of cross section on energy. The Deck-model cross section does not exactly follow a simple power law in lab momentum, but it is well approximated between 50 and 200 GeV/c by  $\sigma \sim p_L^{-0.28}$ . As shown in Fig. 10, this momentum dependence is consistent with the experimental data between 20 and 205 GeV/c.

The Deck model will now be compared in some detail to experimental data<sup>17</sup> at 205 GeV/c. The normalization of the experimental histograms is determined in all cases but one by the cross section reported in Ref. 17:  $(0.68 \pm 0.14)$  mb for 191 events.

Figure 11 shows the distribution in  $W$ , the  $p\pi\pi$  mass. Given the low statistics of the data and the uncertainty in its normalization, there is no discrepancy of note between theory and experiment. The fact that the data have a higher peak than the theory could either be due to the presence of unresolved narrow bumps in the data or to an error in normalization. Two-particle spectra are shown in Fig. 12. Again, agreement between theory and experiment is excellent.

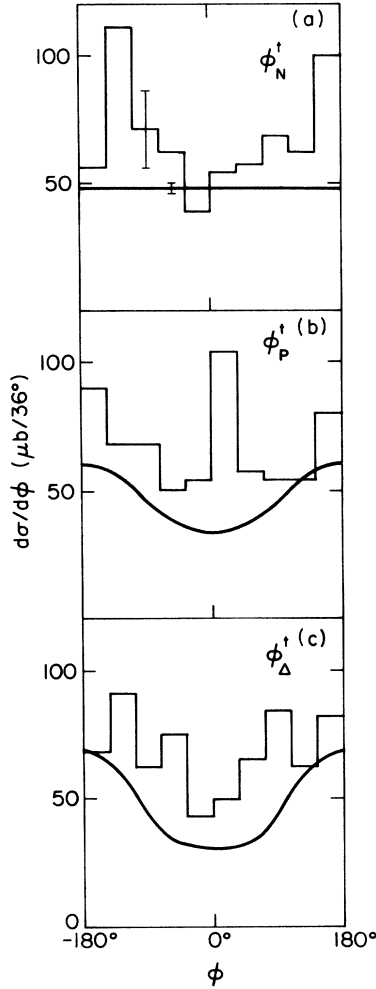


FIG. 14. Azimuthal angular distributions in the  $t$ -channel coordinate system of (a) the normal to the  $p\pi\pi$  system, (b) the proton, (c) the  $(p\pi^+)$  system, for the reaction  $pp \rightarrow pp\pi^+\pi^-$  at 205 GeV. The experimental histograms are taken from Ref. 17.

Angular variables will now be examined. The momentum transfer between the  $p\pi\pi$  system and the associated incident proton is displayed in Fig. 13. The scale of the experimental points has been taken directly from the figure in Ref. 17. Given the results which have been summarized in Table I for the reaction  $p\bar{p} \rightarrow p\bar{p}\pi^+\pi^-$ , we are a bit skeptical of the excellent agreement between theoretical and experimental  $t$  distributions. Previously, discrepancies appeared when  $t$  distributions were examined in limited regions of  $W$ . It seems reasonable to suppose that the same effect is present here, and that the agreement is only obtained by integrating over  $W$ . In addition, there are probably discrepancies between theory and experiment in the azimuthal distributions displayed in Fig. 14.

TABLE II. Deviation from isotropy of theoretical azimuthal distributions measured in  $t$ -channel and  $s$ -channel coordinate systems for the reaction  $pp \rightarrow pp\pi^+\pi^-$ .

Angle (rad)	$(\sigma_{\max} - \sigma_{\min})/\sigma_{\max}$	
	$t$ channel	$s$ channel
$\phi_N$	0	0.50
$\phi_P$	0.44	0.78
$\phi_\Delta$	0.56	0.78

These angles are defined in the  $p\pi\pi$  center-of-mass system with the  $z$  axis in the direction of the incident proton and the recoil proton in the  $x-z$  plane. As pointed out in Ref. 17, all three distributions must be isotropic if  $t$ -channel helicity is conserved. The data are reasonably consistent with isotropy, whereas the calculated distributions are not. Although the statistics of the data are poor enough so that agreement between theory and experiment cannot be absolutely ruled out, the problems encountered earlier with angular variables lead us to believe that there is probably a real discrepancy here.

The same azimuthal angles can be defined in the over-all center-of-mass system, with the  $z$  axis in the  $p\pi\pi$  direction. These distributions would be flat if  $s$ -channel helicity were conserved. Table II shows that there is less isotropy in the  $s$ -channel angles than the  $t$  channel, and thus that the Deck model is closer to  $t$ -channel helicity con-

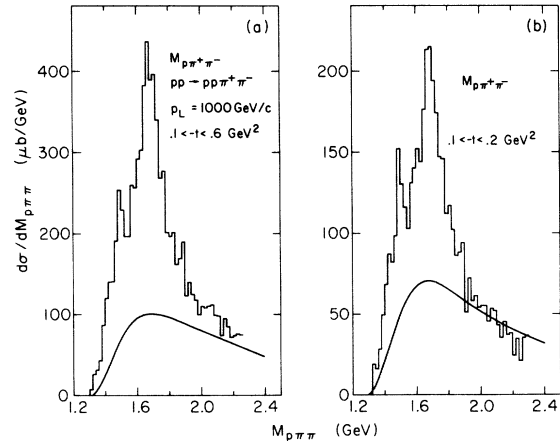


FIG. 15. Distribution in  $W = M_{p\pi\pi}$  for the reaction  $pp \rightarrow pp\pi^+\pi^-$  at 1000 GeV/c. The experimental data are from Ref. 22, and have been corrected for acceptance. The normalization of the experimental cross section has been deduced as best we can from the figures in Ref. 22, and we feel that there is an uncertainty of about 10% in this process. In addition, Ref. 22 quotes an uncertainty of  $\pm 20\%$  in the over-all normalization of their data.

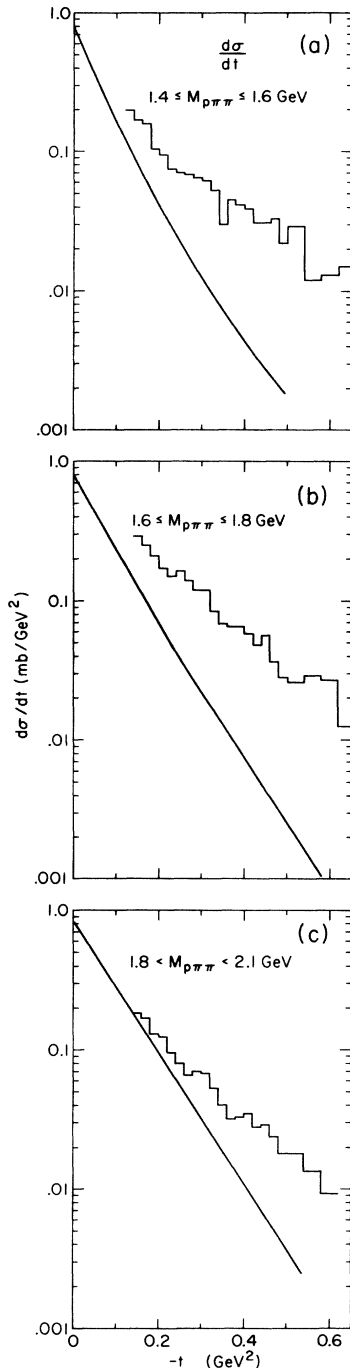


FIG. 16. Momentum transfer,  $t$ , for the reaction  $pp \rightarrow p(p\pi^+p^-)$  at 1000 GeV/c. The experimental points are taken from Ref. 22.

serving than  $s$  channel. This situation is qualitatively similar to that found in both Deck model<sup>2</sup> and experiment<sup>21</sup> for the reaction  $\pi p \rightarrow 3\pi p$ .

Experimental data<sup>22</sup> on the reaction  $pp \rightarrow pp\pi^+\pi^-$  are also available from the CERN ISR at an effective lab momentum of 1000 GeV/c. The distributions in

$W$ , the mass of the  $p\pi\pi$  system, resulting from our Deck model are compared to experimental data in Fig. 15, for two ranges of  $t$ . Acceptance corrections (as shown in Ref. 22) have been applied to the data. It should be emphasized that the region of  $t$  ( $-t \leq 0.1$  GeV<sup>2</sup>) which has dominated  $d\sigma/dW$  in previous figures has been excluded in Fig. 15. Thus, it is not entirely surprising that the comparison of our model with data looks somewhat different in this case. It appears that for  $W < 1.8$  GeV<sup>2</sup> there are large resonant contributions, which in Ref. 22 are identified with the  $N(1520)$  and  $N(1688)$ . In fact, our Deck-model prediction has approximately the same size as the fourth-order polynomial fit to background reported in Ref. 22. For  $W > 1.8$  GeV our model agrees with the data within the uncertainty of experimental normalization.

Distributions in momentum transfer to the  $p\pi\pi$  system,  $t$ , are displayed in Fig. 16 for three regions of  $W$ . In all three regions of  $W$ , the data are seen to be decreasing less steeply with  $-t$  than in our model, particularly for  $-t \gtrsim 0.3$  GeV<sup>2</sup>. (This region of  $t$ , of course, has not been examined in our previous displays of  $t$  distributions, cf. Table I and Fig. 13.) One might suppose that the diffractive production of resonances in this region has a substantially different  $t$  dependence from the elastic scattering cross section which determines the  $t$  dependence of our Deck model, but there is certainly no clear evidence that these discrepancies may be entirely ascribed to this cause.

#### V. DECK MODEL FOR THE INCLUSIVE REACTION $pp \rightarrow pX$

Our attempts to extend the Reggeized Deck model to the inclusive reaction have had only a qualitative success, as opposed to the semiquantitative success of the previous sections. Nevertheless, it seems worthwhile to present here our results for the inclusive process based on the same parametrization as used for the exclusive reaction  $pp \rightarrow pp\pi\pi$ . In order to extend the model to the inclusive reaction we must assume that the unknown reaction products in  $X$  are produced by the pion exchange diagram of the Deck model. It is also necessary to neglect interference terms between diagrams in which the final-state pions are emitted at interchanged positions along the multiperipheral chain.

The analog for the inclusive reaction of the diagrams I and II of Fig. 1 studied above for  $pp \rightarrow pp\pi\pi$  is shown in Fig. 17(a). The blob on the bottom of this diagram represents elastic  $\pi N$  scattering; the blob on the top represents  $\pi N \rightarrow$  anything. The

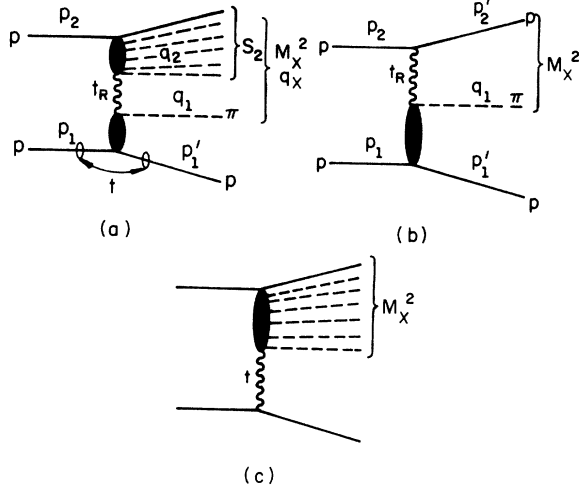


FIG. 17. Diagrams for the inclusive reaction  $pp \rightarrow pX$ . Wiggly lines represent Reggeized pion exchanges. Shaded blobs represent full amplitudes.

cross section resulting from this diagram will have, then, a factor  $|\mathfrak{M}^{\pi N}|^2$  corresponding to the blob on the bottom and a factor of

$$\begin{aligned} \frac{1}{(2\pi)^6} \int \frac{d^3q_1}{2E_1} \int \frac{d^3p'_1}{2E_{p'_1}} &= \frac{1}{(2\pi)^6} \int dM_X^2 \int ds_2 \int d^4q_X \int d^4p'_1 \delta(q_X^2 - M_X^2) \delta(p_1'^2 - m_p^2) \delta^4(p'_1 + q_X - P) \\ &\times \int d^4q_1 \int d^4q_2 \delta(q_1^2 - m_\pi^2) \delta(q_2^2 - s_2) \delta^4(q_1 + q_2 - q_X) \\ &= \frac{1}{(2\pi)^6} \int dM_X^2 \int ds_2 \frac{|\vec{q}_X|}{4/s} \int d\Omega \frac{|\vec{q}_1|}{4M_X} \int d\Omega_1, \end{aligned} \quad (15)$$

where we have evaluated successive two-body phase spaces in their appropriate center-of-mass (c.m.) systems [the c.m. system of  $\vec{q}_X$  and  $\vec{p}'_1$  for  $(|\vec{q}_X|/4\sqrt{s}) \int d\Omega$ ; the c.m. system of  $\vec{q}_1$  and  $\vec{q}_2$  for  $(|\vec{q}_1|/4M_X) \int d\Omega_1$ ]. The integral over the solid angle in the over-all center-of-mass system can be related to an integral over  $t$ :

$$d\Omega = 2\pi d(\cos\theta) = (\pi/p_1 p'_1) dt, \quad (16)$$

with three momenta  $p_1$  and  $p'_1 = |\vec{q}_X|$  evaluated in the over-all c.m. system. Dividing by some additional phase-space factors  $2E_{p_1} \cdot 2E_{p_2}$  and the initial flux  $p_1 \sqrt{s} / E_{p_1} E_{p_2}$  and combining results, we obtain for the cross section for the inclusive reaction the formula

$$\frac{d\sigma}{dM_X^2 dt} = \frac{1}{(2\pi)^6} \frac{\pi}{32s p_1^2 M_X} \int ds_2 |\vec{q}_1| \int d\Omega_1 \text{Im} \mathfrak{M}^{\pi N}(\text{forward}) \left( \frac{s' - u'}{2s_0} \right)^{2\alpha_\pi(t_R)} \frac{1}{(t_R - m_\pi^2)^2} |\mathfrak{M}^{\pi N}|^2. \quad (17)$$

(Here we have evaluated  $|\vec{q}_1| \int d\Omega_1$  in the c.m. system of  $\vec{q}_1$  and  $\vec{q}_2$ .) This is the inclusive cross section for the production of the system  $X$  in Fig. 15(a) consisting of the pion of momentum  $q_1$  plus anything produced in the collision of the exchanged pion and the proton of momentum  $p_2$ . A formula of this type was first given by Sorenson.<sup>23</sup>

For  $\text{Im} \mathfrak{M}^{\pi N}(\text{forward})$  in Eq. (17) we use on-shell experimental data. This does not include the contribution from the diagram in Fig. 17(b), in which the system of mass squared  $s_2$  [referring to Fig. 17(a)] is a single nucleon. We can obtain the result for the diagram of Fig. 17(b) by the replacement

$$\text{Im} \mathfrak{M}^{\pi N}(\text{forward}) \rightarrow \pi \delta(s_2 - m_p^2) g^2 (-t_R) \quad (18)$$

in the formula (17), where  $g$  is the  $\pi N$  coupling constant and the factor  $(-t_R)$  is the well-known one which

$$2 \text{Im} \mathfrak{M}^{\pi N}(\text{forward}) = \sum_n (2\pi)^4 \delta \left( P - \sum_{i=1}^n p_i \right) \frac{|M_{2 \rightarrow n}|^2}{\prod_{i=1}^n 2E_i} \quad (12)$$

corresponding to the blob on the top. Corresponding to the Reggeized pion exchange we use a factor

$$\left( \frac{s' - u'}{2s_0} \right)^{2\alpha_\pi(t_R)} \frac{1}{(t_R - m_\pi^2)^2}, \quad (13)$$

with  $s_0 = 1.0 \text{ GeV}^2$  and

$$\frac{s' - u'}{2} = M_X^2 + \frac{1}{2} (-m_\pi^2 - m_p^2 + t_R - s_2 - t). \quad (14)$$

In this formula the particles emerging from the blob at the top of Fig. 17(a), with (total mass)<sup>2</sup> =  $s_2$ , are treated as a single composite particle. As discussed in Sec. II and Ref. 1, this procedure seems reasonable since  $s_2$  will be constrained to the resonance region,  $s_2 < 4.0 \text{ GeV}^2$ .

The phase space for the final state indicated in Fig. 17(a), aside from that already incorporated on the right-hand side of Eq. (12), can be written in the form

arises when one performs the spin sum for the protons. Thus, for the diagram of Fig. 17(b) we obtain the result

$$\frac{d\sigma}{dM_X^2 dt} = \frac{1}{(2\pi)^6} \frac{\pi}{32s p_1^2 M_X} (\pi g^2) |\tilde{q}_1| \int d\Omega_1 \left( \frac{s' - u'}{2s_0} \right)^{2\alpha_\pi(t_R)} \frac{-t_R}{(t_R^2 - m_\pi^2)^2} |\mathfrak{M}^{\pi N}|^2. \quad (19)$$

Finally we considered the pion-exchange diagram of Fig. 17(c), which gives a contribution

$$\frac{d\sigma}{dM_X^2 dt} = \frac{1}{4\pi} \frac{g^2}{4\pi} \frac{1}{4p_1^2 s} \frac{-t}{(t - m_\pi^2)^2} \text{Im} \mathfrak{M}^{\pi N}(\text{forward}). \quad (20)$$

In these formulas  $|\mathfrak{M}^{\pi N}|^2$  is summed and averaged over appropriate spin states, and the appropriate sum must also be performed over the various allowed pion and nucleon charge states.

The results of some numerical calculations based on the above formulas and using a numerical integration scheme similar to that of Ref. 15 are given in Figs. 18 and 19. On the figures are also given the data of the gas jet target group from Fermilab obtained in the experiments using a special slit to improve the resolution.<sup>24</sup> The curves with the large bumps peaking at  $M_X^2 = 1.8 \text{ GeV}^2$  in Fig. 18 are the contribution from the diagram of Fig. 17(b), i.e., formula (19), multiplied by a factor of 0.38. The curves with the small broad bumps peaking at  $M_X^2 \approx 2.5\text{--}3.0 \text{ GeV}^2$  are the contribution from the diagram of Fig. 17(a), i.e., formula (17). The contributions from the diagram of Fig. 17(c), i.e., formula (20), are negligible in the low  $M_X^2$  region and are not plotted in Fig. 18. In Fig. 19 the slope parameters describing the  $t$  dependence are given for the two diagrams 17(a) and 17(b) and for the data.

It is immediately apparent that the calculations do not agree with the data. At best there is perhaps a qualitative explanation for some effects seen in the data. We can make the following comments:

(a) With the parametrization used in Eq. (19) the contribution of diagram 17(b) is much too large; in fact, 0.38 times the calculated values are plotted in Fig. 18. Moreover, the peaks in the theoretical  $M_X^2$  distributions occur at lower values of  $M_X^2$  than in the data.

(b) From Fig. 19 we see that while the slope parameter  $b$  does decrease with increasing  $M_X^2$  in the model, the tendency is not nearly as pronounced as in the data. As discussed above—see Fig. 9, Table I, the discussion in Sec. III, and the work of Miettinen and Pirilä<sup>25</sup>—this seems to be a general problem of Deck models.

(c) We tried, without much success, to find a form factor  $F(t_R)$  which was a function only of  $t_R$  and not  $t$ , which would remove the discrepancies

discussed above under (a) and (b). An exponential form factor  $F(t_R) = \exp[a(t_R - m_\pi^2)]$  with  $a \approx 3.5 \text{ GeV}^{-2}$  will decrease the over-all size of the contribution of Fig. 17(b) to a reasonable value. However, the peak in the  $M_X^2$  distribution now occurs at even smaller values of  $M_X^2$  than that of the curves in Fig. 18—at about  $M_X^2 \approx 1.5 \text{ GeV}^2$ . The curve for the slope parameter  $b$ , Fig. 19, has about the right shape, but is too low by about 5

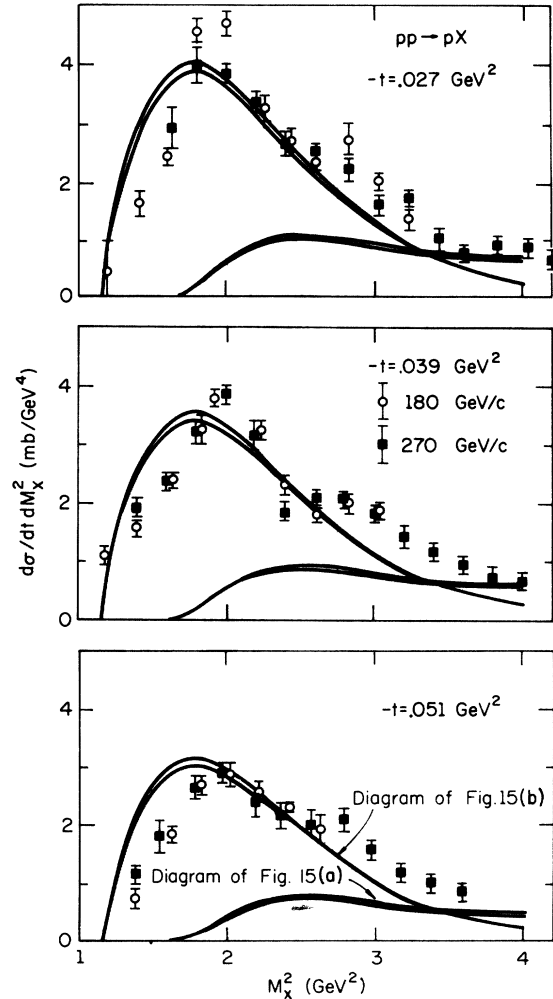


FIG. 18. Distributions in  $M_X^2$  for the reaction  $pp \rightarrow pX$  for three values of  $t$ . The theoretical curves are calculated separately for the two diagrams (a) and (b) of Fig. 15. In each pair of theoretical curves the upper curve was calculated at  $p_L = 180 \text{ GeV}/c$ , the lower curve at  $p_L = 270 \text{ GeV}/c$ . The data are taken from Ref. 24.

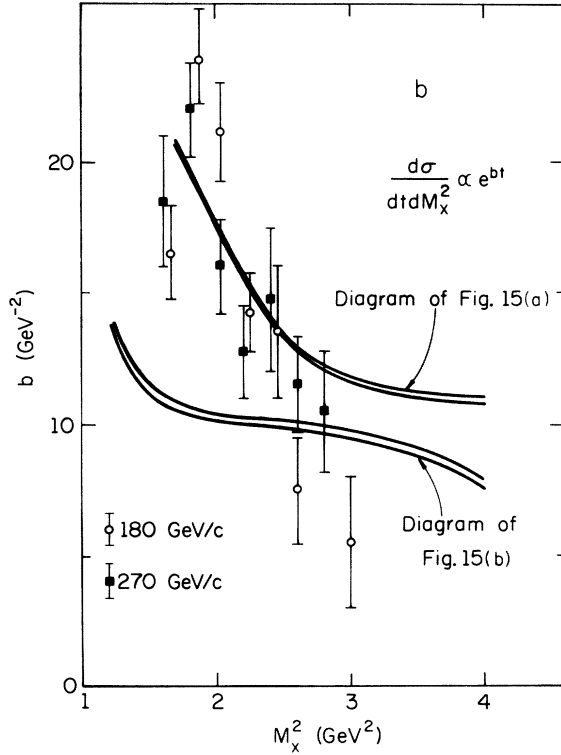


FIG. 19. Slope  $b$  of the cross section  $d\sigma/(dt dM_X^2) \propto e^{bt}$  for the reaction  $pp \rightarrow pX$ . The theoretical curves are calculated separately for the two diagrams (a) and (b) of Fig. 17. In each pair of theoretical curves the lower curve was calculated at  $p_L = 180$  GeV/c and the upper curve at  $p_L = 270$  GeV/c. The data are taken from Ref. 24.

GeV<sup>-2</sup>. In order to move the peak in the  $M_X^2$  distribution to larger values we need a form factor with contributions from large  $t_R$ . To preserve the correct over-all size we thus need a form factor which drops quickly and flattens out; one such is  $F(t_R) = 0.38$ , used in plotting Figs. 18 and 19. In order to push the position of the peak to even higher  $M_X^2$  we need a form factor which drops rapidly and then rises with increasing  $|t_R|$ . The latter possibility leads to a curve for the slope parameter even flatter than that of Fig. 19.

(d) Tsarev *et al.*<sup>26,27</sup> have obtained a much better fit to the data using a formula similar to Eq. (19). In addition to a slightly different Reggeization prescription [they use  $(M_X^2 - m_\rho^2)^{\alpha_\pi}$  in place of  $[\frac{1}{2}(s' - u')]^{\alpha_\pi}$ —see Eqs. (13), (14)], these authors include form factors  $F_1(t_R) = \exp[2 \text{ GeV}^{-2}(t_R - m_\pi^2)]$  and  $F_2(t) = \exp[3 \text{ GeV}^{-2}(t - m_\pi^2)]$ . The form factor  $F_1(t_R)$  seems plausible to us, but the other form factor  $F_2(t)$  seems rather ad hoc. In any event, we wish to emphasize here that the parametrization which we found successful in several Deck

model calculations is unsuccessful for the diagram of Fig. 17(b).

(e) The diagram of Fig. 17(a) which is dominated by  $pp \rightarrow p\Delta\pi$ , gives rise to a small bump with a broad maximum in  $M_X^2$  between 2.5 GeV<sup>2</sup> and 3.0 GeV<sup>2</sup>—see Fig. 18. The Deck effect involved in the diagram of Fig. 17(a) is very similar to that discussed for  $p\bar{p} \rightarrow p\bar{p}\pi\pi$  in earlier sections of this paper and to the Deck effect for  $\pi p \rightarrow \pi\pi p$  discussed in earlier work by our group.<sup>1</sup> As in these other calculations, the calculation of the diagram of Fig. 17(a) seems to produce results of a reasonable size without the introduction of any arbitrary form factors. Unfortunately, the Deck effect of diagram 17(a) is swamped by the larger effects of diagram 17(b). Nevertheless, it seems possible that when the smaller Deck effect of diagram 17(a) is added to the dominant  $pp \rightarrow pN\pi$  diagram 17(b), it could give rise to a shoulder of the sort which can be seen in the data plotted in Fig. 18.

Thus, it seems possible that the main features of low  $M_X^2$  diffraction dissociation are due to the Deck effect, the larger bump due to  $pp \rightarrow pN\pi$  and the shoulder due to  $pp \rightarrow p\Delta\pi$ . A convincing demonstration of this would require at a minimum a unified way of dealing with both diagrams 17(a) and 17(b) with the same parametrization and form factors used in other Deck-model calculations such as  $p\bar{p} \rightarrow p\bar{p}\pi\pi$  and  $\pi p \rightarrow \pi\pi p$ .

## VI. CONCLUSIONS

We have investigated the Deck model for the reactions  $p\bar{p} \rightarrow p\bar{p}\pi^+\pi^-$ ,  $p\bar{p} \rightarrow p\bar{p}\pi^+\pi^-$ , and  $pp \rightarrow pX$  in the kinematic region where low-mass baryonic systems are diffractively produced. This is a continuation of earlier work in AW on the Deck model for the reaction  $\pi p \rightarrow 3\pi p$ . A major reason for the new study was the appearance of new data for the reaction  $p\bar{p} \rightarrow p\bar{p}\pi^+\pi^-$ .

In the exclusive reactions studied, good agreement with data in both shape and normalization is achieved for mass spectra, although it is clear that the data have substantial resonance contributions which are not included in the model. Angular distributions are less well predicted, but it is not obvious which discrepancies are due to problems in the model and which are due to resonances that are simply not included. Some angular distributions are found to be distressingly sensitive to the exact way in which on-shell amplitudes are used. It is, on the other hand, becoming increasingly clear that reasonable modifications of this type of Deck model cannot reproduce the highly peripheral nature of production near threshold, a problem which seems to be common to all Deck mod-

els.

Our calculations of the inclusive reaction indicate that most of low-mass production may be due to the Deck effect in various forms, and that any resonance production in this process is probably a small addition to the Deck effect. Unfortunately, the problems in the Deck model, which are observed but tolerated for four-body final-state exclusive reactions, seem to become more serious for the reaction  $pp \rightarrow pN\pi$ , which is the major component of the inclusive reaction.

We close by adding a few comments of a more general character. There is conflicting evidence for many bumps in nucleon diffractive dissociation. In the recent review of Mukhin and Tsarev<sup>28</sup> evidence is cited for bumps at  $M_X = 1.3, 1.45, 1.47, 1.5, 1.7, \text{ and } 2.2$  GeV. It is clear that the Deck model cannot account for all this complex structure. There are certainly substantial contributions from several resonant states, which are not included in the model. On the other hand, it is equally clear that the Deck model does account for a prominent (or even dominant) background to which the resonant states must be added. This background consists of a large bump peaked at

$M_X^2 \sim 1.8$  GeV and due to  $pp \rightarrow pN\pi$  and a much smaller bump peaked in the region  $M_X^2 \sim 2.5-3.0$  GeV and due mainly to  $pp \rightarrow p\Delta\pi \rightarrow pN\pi\pi$ . It is likely that a complete disentangling of the resonances from the background can be carried out only by performing an amplitude analysis on the data analogous to that performed on the data for  $\pi p \rightarrow 3\pi p$ .<sup>29,30</sup> Such an analysis would hopefully enable one to distinguish true resonances (bumps in specific angular momentum states showing simultaneous variations of magnitude and phase of the type described by the Breit-Wigner formula) from Deck effects (bumps in certain *S*-wave states with no corresponding phase variations).

#### ACKNOWLEDGMENTS

We would like to thank Professor Levine for his permission to use the algebra program ASHMEDAI, and for his kind assistance. We also thank Professor R. D. Sard and A. Snyder for their help in interpreting and presenting the experimental data, and Professor R. L. Schult and Professor D. R. Snider for their useful suggestions.

\*Work supported in part by National Science Foundation Grant No. MPS 73-05103-A01 and Atomic Energy Commission Grant No. AT(11-1)-1195.

- <sup>1</sup>G. Ascoli, R. Cutler, L. M. Jones, U. Kruse, T. Roberts, B. Weinstein, and H. W. Wyld, Jr., *Phys. Rev. D* **9**, 1963 (1974). This reference is referred to as AW in the text.
- <sup>2</sup>Yu. M. Antipov *et al.*, *Nucl. Phys. B* (to be published).
- <sup>3</sup>E. L. Berger *et al.*, *Phys. Rev. Lett.* **20**, 964 (1968).
- <sup>4</sup>E. L. Berger, *Phys. Rev.* **179**, 1567 (1969).
- <sup>5</sup>E. L. Berger, *Phys. Rev. Lett.* **21**, 701 (1968).
- <sup>6</sup>E. Colton, P. E. Schlein, E. Gellert, and G. A. Smith, *Phys. Rev. D* **3**, 1063 (1971).
- <sup>7</sup>E. Colton, Z. Ming Ma, G. A. Smith, and P. E. Schlein, *Phys. Rev. D* **7**, 3267 (1973).
- <sup>8</sup>G. Wolf, *Phys. Rev.* **182**, 1538 (1969).
- <sup>9</sup>L. Brink and S. O. Holmgren, *Phys. Scr.* **8**, 231 (1973).
- <sup>10</sup>K. G. Borekov, A. B. Kaidalov, and L. A. Ponomarev, paper submitted to the Seventeenth International Conference on High Energy Physics, London, 1974 (unpublished). This work contains several references to the Soviet literature on the Deck model. L. A. Ponomarev, Institute of Theoretical and Experimental Physics, Report No. ITEF-77, Moscow, 1974 (unpublished); L. A. Ponomarev, Institute of Theoretical and Experimental Physics, Report No. ITEF-78, Moscow, 1974 (unpublished).
- <sup>11</sup>S. D. Protopopescu *et al.*, *Phys. Rev. D* **7**, 1269 (1973).
- <sup>12</sup>A. Donnachie, R. G. Kirsopp, and C. Lovelace, *Phys. Lett.* **26B**, 161 (1968).
- <sup>13</sup>V. Barger and R. J. N. Phillips, *Phys. Rev.* **187**, 2210 (1969).

- <sup>14</sup>M. J. Levine, AEC Report No. CAR-882-25, 1971 (unpublished).
- <sup>15</sup>G. Ascoli, L. M. Jones, B. Weinstein, and H. W. Wyld, Jr., *Phys. Rev. D* **8**, 3894 (1973).
- <sup>16</sup>The data were taken from the compilation made by G. Ascoli and U. Kruse at the University of Illinois for the purpose of studying the  $A_3$  effect; particular groups of contributors are listed in G. Ascoli *et al.*, *Phys. Rev. D* **7**, 699 (1973).
- <sup>17</sup>M. Derrick, B. Musgrave, P. Schreiner, and H. Yuta, *Phys. Rev. D* **9**, 1215 (1974).
- <sup>18</sup>J. D. Hansen *et al.*, CERN Report No. CERN/HERA 70-2, 1970 (unpublished).
- <sup>19</sup>U. Idschok *et al.*, *Nucl. Phys.* **B53**, 282 (1973).
- <sup>20</sup>J. G. Rushbrooke *et al.*, *Phys. Rev. D* **4**, 3273 (1971).
- <sup>21</sup>R. Klanner, CERN NP Internal Report No. 73-9, 1973 (unpublished); Y. M. Antipov *et al.*, *Nucl. Phys.* **B63**, 153 (1973); G. Ascoli *et al.*, *Phys. Rev. Lett.* **26**, 929 (1971).
- <sup>22</sup>R. Webb *et al.*, *Phys. Lett.* **55B**, 331 (1975).
- <sup>23</sup>C. Sorensen, *Phys. Rev. D* **6**, 2554 (1972).
- <sup>24</sup>Y. Akimov *et al.*, NAL Report No. NAL-Conf-74/66 Exp, Rockefeller University Report No. COO-2232A-5, University of Rochester Report No. COO-3065-88 (UR-495), submitted to the Seventeenth International Conference on High Energy Physics, London, 1974 (unpublished); *Phys. Rev. Lett.* **35**, 763 (1975); **35**, 766 (1975).
- <sup>25</sup>H. I. Miettinen and P. Pirilä, *Phys. Lett.* **40B**, 127 (1972).
- <sup>26</sup>V. A. Tsarev, *Phys. Rev. D* **11**, 1864 (1975).
- <sup>27</sup>Y. Akimov *et al.*, Fermilab Report No. Fermilab-

Conf-74/79-THY/EXP, submitted to the Seventeenth International Conference on High Energy Physics, London, 1974 (unpublished).

<sup>28</sup>S. V. Mukhin and V. A. Tsarev, in *Particles and Fields-1974*, proceedings of the Williamsburg meeting of the Division of Particles and Fields of the American

Physical Society, edited by C. E. Carlson (A.I.P., N. Y., 1974), p. 263.

<sup>29</sup>Yu. M. Antipov *et al.*, Nucl. Phys. B63, 153 (1973).

<sup>30</sup>See also the suggestion by G. C. Fox, Phys. Rev. D 9, 3196 (1974).